European Journal of Pharmaceutics and Biopharmaceutics 71 (2009) 100–108

Contents lists available at ScienceDirect

European Journal of Pharmaceutics and Biopharmaceutics

journal homepage: www.elsevier.com/locate/ejpb

Research paper

Understanding the solid-state forms of fenofibrate – A spectroscopic and computational study

Andrea Heinz [a,b,c,*], Keith C. Gordon [d], Cushla M. McGoverin [d], Thomas Rades [a], Clare J. Strachan [c]

[a] School of Pharmacy, University of Otago, Dunedin, New Zealand
[b] Division of Pharmaceutical Technology, University of Helsinki, Helsinki, Finland
[c] Drug Discovery and Development Technology Center (DDTC), University of Helsinki, Helsinki, Finland
[d] Department of Chemistry, University of Otago, Dunedin, New Zealand

ARTICLE INFO

Article history:
Received 24 February 2008
Accepted in revised form 21 May 2008
Available online 12 June 2008

Keywords:
Density functional theory
Infrared spectroscopy
Raman spectroscopy
Principal component analysis
Metastable
Recrystallization
Amorphous
Polymorphism

ABSTRACT

The aim of this study was to investigate the structure of different solid-state forms of fenofibrate, a drug that lacks strong intermolecular interactions such as hydrogen bonding. In addition to a structural analysis of crystalline and amorphous fenofibrate using infrared and Raman spectroscopy combined with density functional theory calculations [B3LYP 6-31G(d)], solid-state changes that occur upon recrystallization of amorphous fenofibrate were monitored and described using *in situ* Raman spectroscopy. A comparison of the calculated vibrational spectra of a fenofibrate monomer and two dimer structures with the experimental vibrational spectra of crystalline and amorphous fenofibrate revealed conformational differences in the orientation of the two benzyl rings in the fenofibrate molecule and structural differences between the different solid-state forms in aliphatic parts of the drug molecule. The spectroscopic analysis suggests that non-hydrogen-bonded drug molecules are likely to exhibit more random molecular orientations and conformations in the amorphous phase since the weak intermolecular interactions that occur between such molecules can easily be disrupted. *In situ* Raman spectroscopy and multivariate analysis revealed multiple solid-state forms of fenofibrate, including the metastable crystalline form II, which were structurally analyzed with reference to the quantum chemical calculations. Overall, the study showed that vibrational spectroscopy, multivariate analysis, and quantum chemical modeling are well suited to investigate and characterize the structure of drug substances that exhibit only small structural differences between different solid-state forms.

1. Introduction

Pharmaceutical solids can exist in various solid-state forms which are classified in terms of molecular structure and composition. Crystalline materials are characterized by orientational and positional long-range order in all three dimensions of space. Even though amorphous materials lack long-range order, they may exhibit short-range order which involves interactions between neighboring molecules, such as the formation of dimers [1]. The diversity of solid-state forms of the same compound is based on differences in non-covalent interactions between neighboring molecules and may additionally be associated with changes in molecular conformation. Of the various interactions, hydrogen bonding plays an important role. Other non-covalent attractive forces include van der Waals interactions such as π–π stacking and mainly depend on dipole moments, polarizability, and electronic distribution in the molecules [2,3]. Based on possible molecular interactions and/or conformations, crystalline materials may exist in different polymorphic forms.

Depending on the solid-state form of a pharmaceutical substance, differences in a range of properties, such as morphology, density, stability, melting point, and solubility, may occur. These differences, in turn, may influence the bioavailability, processability, as well as chemical and physical stabilities of the drug. Usually the pharmaceutical solid is manufactured in a stable crystalline form because the amorphous form tends to convert to the crystalline form due to its thermodynamic instability. However, despite this disadvantage, the amorphous state has attracted considerable interest in recent years in the formulation of poorly soluble compounds. The higher molecular mobility of amorphous materials, for instance, may improve the solubility and dissolution rate of the pharmaceutical compound and, thus, facilitate the gastrointestinal absorption of the active drug [4–6]. Whichever solid-state form is chosen, to ensure reproducible quality and efficacy of the pharmaceutical product, it is necessary

* Corresponding author. Solid State Research Group, School of Pharmacy, University of Otago, 18 Frederick Street, Dunedin, New Zealand. Tel.: +64 3 479 5285; fax: +64 3 479 7034.
E-mail address: andrea.heinz@stonebow.otago.ac.nz (A. Heinz).

0939-6411/$ - see front matter © 2008 Elsevier B.V. All rights reserved.
doi:10.1016/j.ejpb.2008.05.030

to comprehensively characterize solid-state forms of a drug and closely monitor solid-state changes that may occur during processing, including recrystallization phenomena and polymorphic transitions.

A range of analytical techniques are available for the physical characterization of crystalline and amorphous compounds [4,7]. X-ray powder diffraction (XRPD), optical microscopy, and thermal methods including differential scanning calorimetry (DSC) and thermogravimetric analysis (TGA), for instance, are utilized to characterize the particulate level [8]. Molecular-level characterization can be carried out using solid-state nuclear magnetic resonance spectroscopy and vibrational spectroscopy, namely, Fourier transform mid-infrared (FTIR), near-infrared (NIR), Raman, and terahertz spectroscopies [1,2,4,9]. Vibrational spectroscopy has become popular to characterize and quantify various solid-state forms of drugs including polymorphs [10–15], solvates [16], amorphous materials [17–19], and salts [20]. However, to gain molecular-level information on solid-state structure from vibrational spectral analysis, the spectral bands of interest must be assigned to the correct molecular vibrations. For pharmaceutical compounds, this is often very challenging. Quantum mechanical calculations, which have only recently been adopted for solid-state analysis in the pharmaceutical setting, are an invaluable tool for interpreting vibrational spectra [21–24]. Together with vibrational spectroscopy, quantum chemical calculations have, for example, been used to analyze conformational differences between the carbamazepine polymorphs form I and form III [21,25], to investigate hydrogen bonding in anhydrate and hydrate forms of theophylline, caffeine, and theobromine [26], to study structural differences between crystalline γ-indomethacin and the amorphous form created by quench-melting γ-indomethacin [22], and to gain insight into the structure of amorphous carbamazepine [27]. It could be shown that both indomethacin and carbamazepine exist predominantly as hydrogen-bonded dimers in the amorphous form.

Spectroscopic techniques have become popular to investigate solid-state transformations since they are rapid, nondestructive and provide molecular-level information. Studies have investigated, for instance, the solid-state forms that appear during isothermal dehydration of piroxicam and carbamazepine hydrate forms using *in situ* NIR and Raman spectroscopies [28] or the solvent-mediated phase transformations of theophylline and nitrofurantoin using *in situ* Raman spectroscopy [29]. Multivariate methods, such as principal component analysis (PCA), have shown to be useful tools to interpret the spectral changes in these cases as they visualize spectral variation in a way that makes it possible to better detect and understand solid-state conversions [28,30–32].

To our knowledge there has never been a study that combines spectroscopy, quantum mechanical calculations, and multivariate analysis for physicochemical analysis of a pharmaceutical compound. In this study, the combination of these techniques was used to investigate the solid-state structure and recrystallization behavior of the model drug fenofibrate. Fenofibrate exhibits polymorphism and is known to exist in two polymorphs, the stable crystalline form I [33] and the metastable form II which has only recently been reported [34]. Fenofibrate is an interesting model drug that is challenging for solid-state analysis by vibrational spectroscopy because it lacks hydrogen-bond donating groups and, hence, prohibits hydrogen bonding to other fenofibrate molecules. The aim of this work was to obtain a deeper understanding of the structure of different solid-state forms of fenofibrate and the solid-state conversions between these forms during recrystallization of amorphous fenofibrate by combining vibrational spectroscopy with quantum mechanical calculations and multivariate analysis.

2. Materials and methods

2.1. Materials

Fenofibrate is known to exist in two polymorphs, the stable form I and the metastable form II [34]. Form I crystallizes in the centrosymmetric triclinic space group $P\bar{1}$ [33]. The crystalline form I of fenofibrate (Fig. 1) was obtained from Sigma–Aldrich, Inc. (St. Louis, MO, USA) and was analyzed as received. Amorphous fenofibrate was prepared by melting the crystalline form I on an aluminum pan in a moisture analyzer (MA 100, Sartorius AG, Göttingen, Germany) at 80 °C [35]. The melt was adjusted to ambient temperature in a desiccator over phosphorus pentoxide to prevent atmospheric moisture condensation on the sample. The amorphous samples were analyzed directly after preparation.

2.2. Analytical techniques

2.2.1. X-ray powder diffraction

XRPD was used to confirm the solid state of crystalline and amorphous fenofibrate. The diffraction patterns were recorded using a theta–theta X-ray powder diffractometer (D8 Advance, Bruker AXS GmbH, Karlsruhe, Germany) equipped with Göbel mirror bent multilayer optics. Measurements were performed in symmetrical reflection mode with CuKα radiation (λ = 0.15418 nm) at 40 kV and 40 mA. The powder samples were scanned in the angular range of 5° (2θ) to 40° (2θ) with a step size of 0.1° (2θ) and a count time of 5 s per step.

The crystal structure of fenofibrate was verified by comparing the experimental XRPD pattern with the theoretical diffractogram obtained from the Cambridge Crystallographic Data Centre (CCDC) using Mercury software (v. 1.4.2, CCDC, Cambridge, UK). A structure with the reference code TADLIU was used to generate the theoretical diffraction patterns of crystalline fenofibrate [33].

2.2.2. Differential scanning calorimetry

DSC was carried out on a Q100 (TA instruments, New Castle, DE, USA). The samples (3–5 mg) were analyzed in crimped aluminium pans at temperatures between −60 and 100 °C. The heating rate was 10 °C min^{-1} and the nitrogen gas flow 50 ml min^{-1}. The calibration of the instrument was performed using indium as metal standard. The thermograms were analyzed using TA Universal Analysis 2000 software (v. 4.0, TA Instruments).

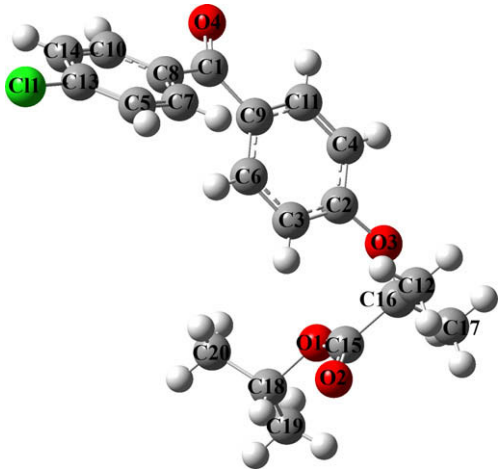

Fig. 1. Molecular structure of fenofibrate with atomic numbering introduced by Henry et al. [33].

2.2.3. Raman spectroscopy

Raman spectra were recorded on a Bruker IFS 55 FT-Raman spectrometer (Bruker Optik, Ettlingen, Germany) in the spectral range between 250 and 3500 cm^{-1} using a diode pumped Nd:YAG laser with an excitation wavelength of 1064 nm at a laser power of 500 mW. Crystalline fenofibrate as obtained from the manufacturer and amorphous fenofibrate were analyzed at room temperature. Temperature-dependent measurements of amorphous fenofibrate samples were carried out between −180 and 90 °C (step size 5 °C) utilizing a variable temperature cell (Specac, Woodstock, GA, USA) and a high stability temperature controller (Specac, Woodstock, GA, USA). Each spectrum was the average of 200 scans. The interferograms were apodized with the Blackman-Harris 4-term function and subjected to Fourier transformation yielding spectra with a resolution of 4 cm^{-1}.

2.2.4. IR spectroscopy

IR spectroscopy was performed on a Bruker Vertex 70 Fourier transform infrared spectrometer (Bruker Optik, Ettlingen, Germany) using an ATR accessory with a single reflection diamond crystal (MIRacle, Pike Technologies, Madison, WI, USA). The spectrometer was equipped with a KBr beamsplitter, an MIR source and a RT-DLaTGS detector. Samples were measured over a wavelength range from 650 to 4000 cm^{-1} and the final spectrum was the mean of 20 scans. The interferograms were apodized with the Blackman-Harris 3-term function and subjected to Fourier transformation yielding spectra with a resolution of 4 cm^{-1}. The ATR spectra were converted to absorbance spectra using OPUS software (v. 5.0, Bruker Optik, Ettlingen, Germany).

2.3. Computational studies

Quantum mechanical calculations were performed on a fenofibrate monomer species and on two dimer structures (one with benzene stacking interaction between the chlorobenzene rings, Fig. 2A, and the other with the isopropyl groups of the aliphatic part of the fenofibrate molecules facing each other, Fig. 2B). The dimers were determined using the crystallographic data as a starting point [33] and each of the structures was identified from differing motifs present in the crystal.

The molecular structure of fenofibrate form I obtained from the Cambridge Crystallographic Database (CCDC, Cambridge, UK) with Conquest software was used as a starting point for the calculations. Density functional theory calculations (B3LYP functional, 6-31G(d) basis set) were performed to first optimize the conformations of the monomer and dimer structures and then to determine the vibrational frequencies and their Raman and IR intensities. The model chemistry was chosen because it has been found to be one of the most reliable methods for modeling medium-sized, conjugated molecules at a reasonable computational cost [36,37]. The calculations were implemented using the Gaussian 03 program [38] which was accessed at CSC – Scientific Computing Limited (Espoo, Finland) through the SOMA2 modeling environment [39,40]. The Raman intensities were determined from the Raman activity for 1064 nm excitation [41] and the calculated frequencies were scaled by a factor of 0.96 [42]. The modes were visualized using GaussView (v. 3.0, Gaussian, Inc., Pittsburgh, PA, USA). Bond lengths, angles, and dihedral angles of the calculated monomer and dimer structures were determined using GaussView and the crystal structure visualization software Mercury.

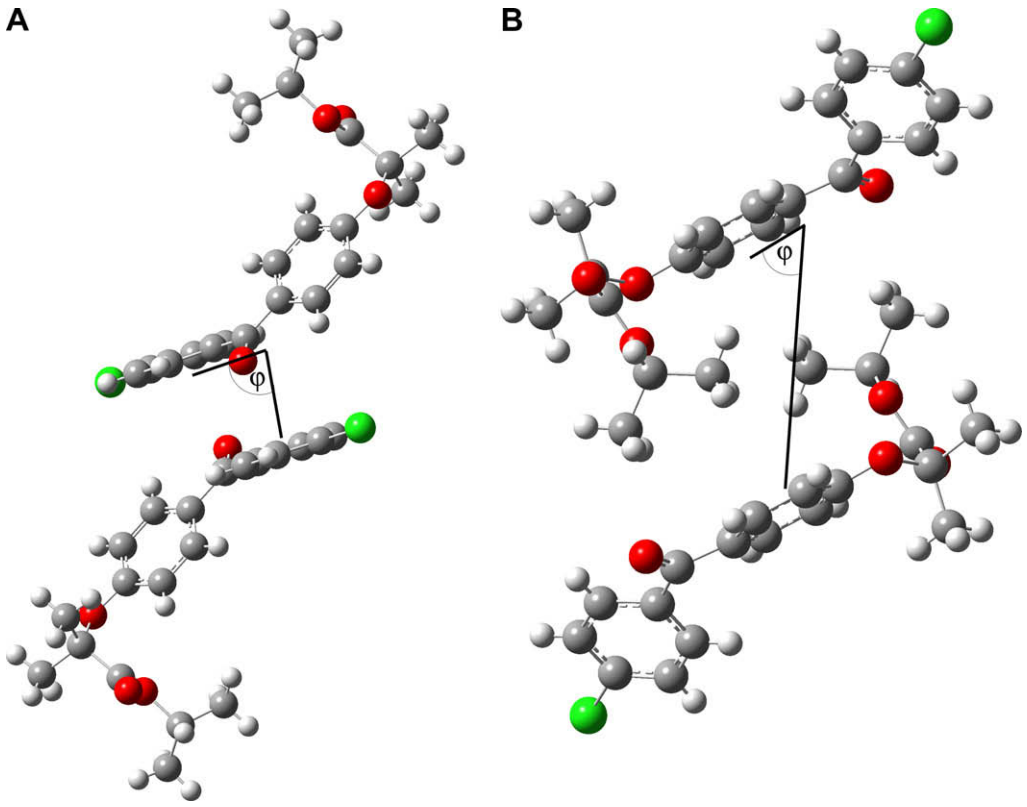

Fig. 2. Molecular structures of the fenofibrate dimers that were used for the quantum mechanical calculations; one with benzene stacking interaction between the aromatic rings (A), the other with aliphatic moieties facing each other (B).

2.4. Multivariate analysis

PCA was used to extract qualitative information from the experimental data obtained by Raman spectroscopy and to visualize the solid-state transformations that occur in the amorphous fenofibrate samples upon heating. All calculations were performed using Simca-P multivariate analysis software (v. 10.5, Umetrics AB, Umeå, Sweden). Prior to PCA the spectral data were subjected to different established pre-treatment and scaling methods and different spectral regions were tested. The best PCA model was obtained when the spectral range between 1050 and 1760 cm^{-1} was chosen and the spectra were standard normal variate (SNV) corrected and mean centered.

3. Results and discussion

3.1. Verification of the solid state of the fenofibrate samples

Fig. 3 shows the experimental X-ray powder diffraction patterns of the crystalline form I and the amorphous form of fenofibrate in comparison with the theoretical diffractogram of the crystalline form I of fenofibrate. Consistent with the theoretical diffractogram the main peaks of crystalline fenofibrate form I were observed at 12° (2θ), 14.5° (2θ), 16.2° (2θ), 16.8° (2θ), and 22.4° (2θ). In the diffractogram of amorphous fenofibrate no distinct peaks can be observed.

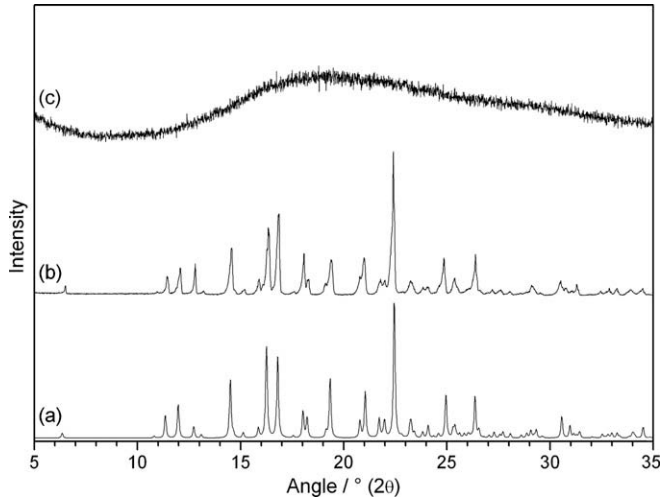

Fig. 3. Theoretical XRPD pattern of crystalline fenofibrate form I with reference code TADLIU (a) compared to the experimental XRPD patterns of crystalline fenofibrate form I (b) and amorphous fenofibrate (c).

3.2. Structural analysis of amorphous and crystalline fenofibrate

3.2.1. Conformational analysis

Henry et al. [33] have carried out crystallographic studies on fenofibrate form I and have introduced a numbering system which was also used in this work (Fig. 1). Upon structural analysis the bond lengths and angles were found to be similar between the fenofibrate molecules of the crystal and the calculated monomer and dimer structures (data not shown). However, differences between experimental and calculated structures were observed with respect to the conformations adopted and the intermolecular distances for the dimers.

Intramolecular structural differences between the experimental and calculated data can, for instance, be found in the conformational orientation of the two benzyl rings of a fenofibrate molecule which are connected via C1 (Fig. 1). The angle between the planes defined by each of the benzyl rings lies at 48.6° in the crystallographic data published by Henry et al. [33], 52.6° in dimer 1, 51.1° in dimer 2, and 49.7° in the fenofibrate monomer (Fig. 4A). Further conformational differences occur in the aliphatic moiety of the fenofibrate molecule. The angle between the planes defined by the benzyl ring (C2, C3, C4, C6, C9, C11) and the aliphatic moiety (C16, C15, O1, C18) was determined to be 85.2° in the crystal structure, 77.5° in dimer 1, 76.1° in dimer 2, and 77.8° in the monomer structure (Fig. 4B).

Comparing different dihedral angles (Table 1) of crystalline form I and the optimized monomer and dimer structures, the main differences are found in dihedral angles around C1 substantiating the finding mentioned before that the orientation of the two benzyl rings is likely to undergo conformational changes. Furthermore, dihedral angles involving the single bonds at O3 (C3–C2–O3–C16 and C4–C2–O3–C16; see Fig. 1) and O1 (C15-O1-C18-C19 and C15-O1-C18-C20; see Fig. 1) in the calculated monomer and dimer structures differ from those in crystalline fenofibrate.

The modeled intermolecular distances and angles are illustrated by comparing the centroids of the benzyl rings. In the crystal structure [33] the stacked chlorobenzene rings (C5, C7, C8, C10, C13, C14; see Fig. 1) are 4.1 Å apart and the angle between the molecules defined by centroid 1-C8-centroid 2 is 96.1°. In dimer 1 the chlorobenzene rings of the two fenofibrate molecules are further apart than in the crystal structure, namely, 5.4 Å, and the angle is, thus, also increased to 113.3°. In dimer 2, where the aliphatic moieties are facing each other, the benzene rings (C2, C3, C4, C6, C9, C11; see Fig. 1) are 8.3 Å apart and the angle between the molecules defined as centroid 1-C9-centroid 2 is 85.6° as compared to

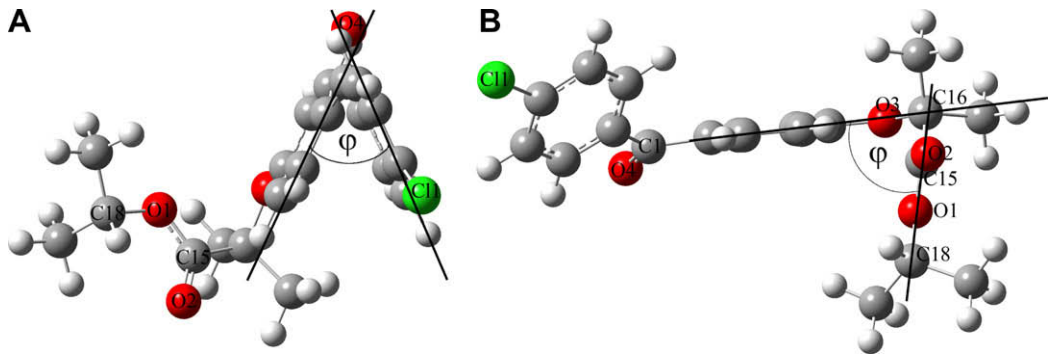

Fig. 4. Angles determined during conformational analysis of different fenofibrate structures. One angle is characterized by the planes defined by each of the benzyl rings (A) and the other is characterized by planes defined by a benzyl ring and the aliphatic moiety (B).

Table 1
Dihedral angles in crystalline fenofibrate form I of the calculated monomer and dimer structures

Bond parameters	Henry et al.[a]	Calculated monomer	Calculated dimer I	Calculated dimer II
	Φ/°	Φ/°	Φ/°	Φ/°
C8–C1–C9–C6	19.4	26.5	21.2	32.0
C7–C8–C1–C9	36.8	32.1	39.9	28.3
C3–C2–O3–C16	−23.3	−5.6	−6.2	−0.9
O3–C16–C15–O1	35.3	40.3	39.1	38.7
C4–C2–O3–C16	157.8	175.5	174.8	179.8
C15–O1–C18–C19	−117.9	−85.0	−85.9	−70.4
C15–O1–C18–C20	122.5	152.1	151.1	170.6

[a] All dihedral angles were determined using GaussView as they have not been published by Henry et al. [33]

the crystal structure where the benzene rings are 7.9 Å apart and the angle is 64.5°.

Overall, the computational studies are consistent with the presence of weak interactions between adjacent molecules as defined by the chosen structural motifs. The conformational analysis suggests that small changes in the conformation of fenofibrate molecules occur predominantly at single bonds which can easily be rotated, thereby affecting in particular the angle between the two aromatic rings and the orientation of the aliphatic part of fenofibrate. Conformational changes upon formation of crystalline and amorphous fenofibrate can hence be expected to occur in these regions of the fenofibrate molecule. Conformational changes may furthermore lead to a change in the distance between two molecules as a result of changes in intermolecular forces.

3.2.2. Spectroscopic analysis

The IR and Raman spectra of crystalline fenofibrate form I and amorphous fenofibrate, as well as those of the optimized monomer and dimer structures, are shown in Fig. 5A and B. Generally, due to the lack of long-range order and the possibility of a range of molecular conformations and intermolecular bonding arrangements, experimental vibrational spectra of amorphous materials exhibit broader merged bands compared to crystalline substances. In this case, band broadening and merging can be observed throughout both the IR and Raman spectra of amorphous fenofibrate, for instance in the carbonyl stretching region between 1650 and 1750 cm^{-1} and in the CH stretching region between 2900 and 3100 cm^{-1}. In addition to changes in band shapes and intensities, band shifts between amorphous and crystalline forms occur. For example, bands that can be assigned to carbonyl stretching vibrations at 1650 and 1728 cm^{-1} in crystalline fenofibrate are shifted to 1656 and 1730 cm^{-1}, respectively, in the IR and Raman spectra of amorphous fenofibrate. Furthermore, a band occurring at 1147 cm^{-1} in the Raman spectrum of crystalline fenofibrate is shifted to 1150 cm^{-1} in amorphous fenofibrate. This band can be assigned to a C16–O3 stretching vibration. Even though some of the specified band shifts are below wavenumber resolution of the spectroscopic techniques, they were found to be consistent and have, thus, been included in the spectroscopic analysis.

The calculated spectra of fenofibrate in the monomer and two dimer forms (Fig. 5A and B) correspond well with the observed spectral data and a comprehensive band assignment has been performed between 1000 and 1800 cm^{-1} (Table 2). Overall, there are very few differences between the monomer and dimer spectra which is most likely due to the lack of hydrogen bonding between fenofibrate molecules. It has been previously described for carbamazepine and indomethacin that intermolecular hydrogen bonding can alter the predicted vibrational spectra of dimer structures compared to those of monomers [22,27]. In the case of fenofibrate, the few bands that are predicted to shift on going from monomer to

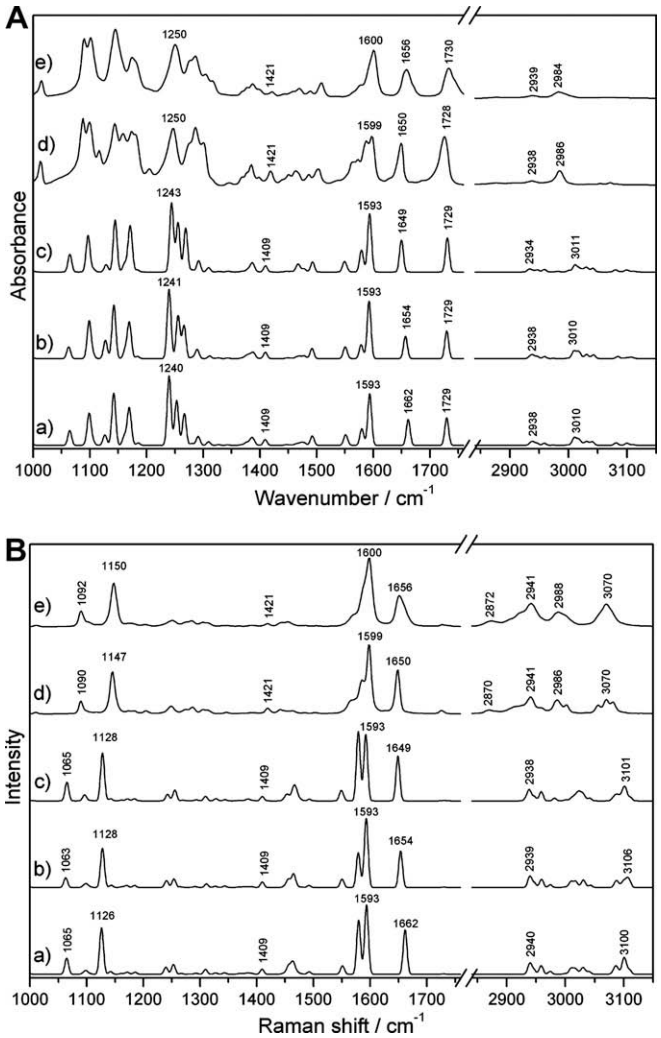

Fig. 5. IR (A) and Raman (B) spectra of a calculated fenofibrate single molecule (a), a calculated dimer structure with benzene stacking interaction between the aromatic rings (b), a calculated dimer structure with aliphatic moieties facing each other (c), experimental crystalline fenofibrate (d), and experimental amorphous fenofibrate (e) in the spectral range between 1000 and 3150 cm^{-1}.

either dimer are correctly predicted. A difference between the experimental vibrational spectra lies in the C=O stretching region around 1650 cm^{-1} where a band, which can be assigned to the C1=O4 carbonyl stretch, is downshifted from 1662 cm^{-1} in the monomer structure to 1654 and 1649 cm^{-1} for the dimers one and two, respectively. This particular band occurs at 1650 and 1656 cm^{-1} in the experimental spectra of crystalline and amorphous fenofibrate, respectively. It is interesting to note that the higher frequency C=O band at 1730 and 1728 cm^{-1} in the experimental spectra for the amorphous and crystalline states, respectively, is predicted at 1729 cm^{-1} in all three calculated structures. This band is due to the C15=O2 stretch.

The comprehensive band assignment has allowed some structural comparison between the crystalline and amorphous forms of fenofibrate. In particular based on the shift of the C1=O4 stretching band, the results of the spectroscopic analysis suggest that crystalline fenofibrate is more similar in its structure to the calculated dimer structures, whereas amorphous fenofibrate shows similarities to both the calculated monomer and dimer structures. Previous computational studies on indomethacin and carbamazepine revealed very little disruption of hydrogen-bonded dimers in the amorphous form [22,27]. This work suggests that

Table 2
IR and Raman wavenumbers, intensities, and vibrational assignments for calculated monomer and dimer structures of fenofibrate and for experimental data of crystalline and amorphous fenofibrate

Calculated monomer ν/cm^{-1} (IR, R intensities[a])	Calculated dimers		Experimental crystalline ν/cm^{-1} (IR, R intensities[a])	Experimental amorphous ν/cm^{-1} (IR, R intensities[a])	Vibrational assignment
	Dimer I ν/cm^{-1} (IR, R intensities[a])	Dimer II ν/cm^{-1} (IR, R intensities[a])			
1065 (21, 23)	1063 (17, 14)	1065 (25, 27)	1090 (67, 25)	1092 (86, 38)	Cl1–C1 stretch, benzene ring deformation (C5, C7, C8, C10, C13, C14)
1099 (47, 6)	1099 (55, 6)	1096 (53, 9)	1101 (89, 10)	1101 (98, 18) R shoulder	O1–C18 stretch, CH3 bending (C19 and C20)
1142 (50, 4)	1143 (77, 3)	1142 (75, 3)	1147 (85, 91)	IR: 1144 (100) R: 1150 (100)	C16–O3 stretch, CH3 bending (C12, C17)
1173 (54, 1)	1171 (53, 3)	1172 (67, 3)	1185 (82, 9)	1180 (merged, 12)	In-plane CH bending in benzene ring (C3H, C4H, C6H, C11H)
1240 (100, 10)	1241 (100, 10)	1243 (100, 10)	1250 (60, 18)	1250 IR (78, 18)	C2-O3 stretch, in-plane benzene ring deformation (C2, C3, C4, C6, C9, C11)
1253 (65, 14)	1254 (62, 13)	1255 (72, 16)	1250 (60, 18)	1250 IR (78, 18)	Asymmetric C8–C1–C9 stretch
1267 (14, 1)	1266 (48, 1)	1270 (63, 1)	1277 (14, 12)	1277 (55, 14)	Asymmetric C16–C15–O1 stretch
1409 (8, 7)	1409 (9, 8)	1409 (9, 7)	1421 (29, 12)	1421 (9, 9)	In-plane benzene ring deformation (C2, C3, C4, C6, C9, C11)
1551 (15, 12)	1550 (17, 12)	1549 (15, 15)	1560 (35, 22) shoulder	1573 (19, 22) shoulder	In-plane benzene ring deformation (C2, C3, C4, C6, C9, C11)
1580 (24, 78)	1579 (20, 50)	1579 (32, 100)	1588 (69, 47)	shoulder	In-plane benzene ring stretch (C5, C7, C8, C10, C13, C14)
1593 (75, 100)	1593 (83, 100)	1593 (84, 96)	1599 (99, 100)	1600 (70, 98)	In-plane benzene ring stretch (C2, C3, C4, C6, C9, C11)
1662 (37, 64)	1654 (32, 53)	1649 (46, 65)	1650 (74, 58)	1656 (42, 45)	C1=O4 stretch
1729 (40, 1)	1729 (49, 1)	1729 (100, 0)	1728 (100, 5)	1730 (44, 5)	C15=O2 stretch

[a] Relative intensities for bands for infrared (IR) and Raman (R) spectra are normalized such that the most intense band in the reported spectral region is 100.

non-hydrogen-bonded drug molecules are likely to exhibit more random molecular orientations and conformations in the amorphous phase since the weak intermolecular interactions that occur between such molecules (e.g., π–π stacking) can easily be disrupted. Furthermore, it is likely that random molecular conformations occur in amorphous fenofibrate when single bonds in the aliphatic part of the drug molecule are rotated. This assumption is substantiated by the fact that band broadening can be observed in the experimental IR and Raman spectra of amorphous fenofibrate and that spectral differences to the crystalline form of fenofibrate are found in regions that can be assigned to aliphatic parts of the drug molecule where bond rotations can occur. Overall, the spectroscopic results give an interesting insight into the structural differences between the crystalline and amorphous forms of a pharmaceutical compound that does not exhibit hydrogen bonding.

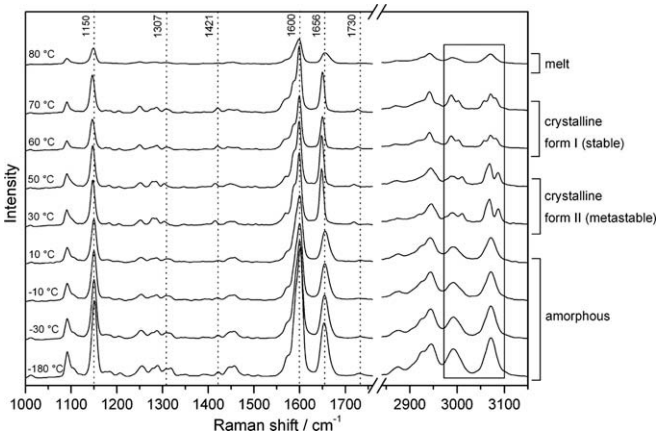

Fig. 6. Selected Raman spectra showing the recrystallization behavior of amorphous fenofibrate in the temperature range between −180 and 80 °C.

3.3. Recrystallization of amorphous fenofibrate

Temperature-dependent Raman spectroscopy was used to investigate the recrystallization behavior of amorphous fenofibrate. Fig. 6 shows selected experimental Raman spectra that were recorded at different temperatures in the temperature range between −180 and 90 °C. Upon heating the amorphous material, significant and distinct band shifts and intensity changes could be observed at 30, 60, and 80 °C, which indicate solid-state conversions at these particular temperatures. A comparison of the experimental Raman spectra with that obtained for crystalline fenofibrate as received from the manufacturer (Fig. 5B) revealed that the crystalline form I of fenofibrate is formed at 60 °C and eventually melts at 80 °C where further changes in the Raman spectra can be observed. The Raman spectra recorded between 30 and 60 °C suggest the presence of a second crystalline solid-state form, metastable form II, whose existence has previously been reported [34].

To further investigate the solid-state of the two crystalline forms that occur between 30 and 80 °C, samples were taken from the variable temperature cell at 40 and 70 °C and analyzed by DSC between 25 and 100 °C. The thermograms were compared to those of amorphous fenofibrate and crystalline fenofibrate form I as received from the manufacturer (Fig. 7). As expected it was found that the sample collected at 70 °C (d) is the crystalline form I of fenofibrate as both this sample and the as-received fenofibrate show a melting endotherm at 80 °C (a and d). This finding is consistent with the results of the temperature-dependent Raman spectroscopic measurements where spectral changes occurred at 80 °C. The thermogram of amorphous fenofibrate (b) shows a recrystallization exotherm with an onset at 30 °C, a melting endotherm of the metastable crystalline form II at 73 °C as has been previously described [34], and a second recrystallization exotherm at 74 °C followed by the melting endotherm of crystalline fenofibrate form I at 80 °C. The sample collected at 40 °C (c) was assumed to contain the metastable crystalline form II and showed a melting endotherm at 73 °C which proves the presence of this solid-state form. Similar to the amorphous sample, metastable form II showed a recrystallization endotherm at 74 °C and subsequent melting of crystalline form I at 80 °C.

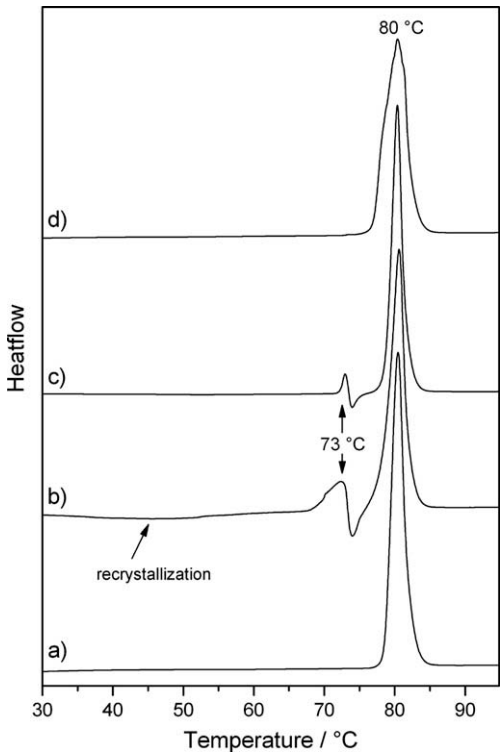

Fig. 7. DSC thermograms of crystalline fenofibrate form I as received from the manufacturer (a), amorphous fenofibrate (b), crystalline fenofibrate form II obtained during temperature-dependent Raman spectroscopy at 40 °C (c), and crystalline fenofibrate form I obtained at 70 °C (d).

The main spectral differences between the different solid-state forms of fenofibrate that are visible in the experimental Raman spectra are summarized in Table 3. Changes were found in bands which occur at 1150, 1307, 1421, 1600, 1656, and 1730 cm^{-1} in the Raman spectra of amorphous fenofibrate and change position upon crystallization to the metastable crystalline form II and stable crystalline form I (Fig. 6). These bands can be assigned to the C16–O3 stretch (1150 cm^{-1}), aromatic stretching and deformation vibrations (1307, 1421, 1600 cm^{-1}), and carbonyl stretching vibrations (1656, 1730 cm^{-1}). Interestingly, all of the above-mentioned bands downshift during crystallization to the metastable form II. The largest changes in band positions are the C15=O2 stretch at 1730 cm^{-1} in the amorphous form that shifts to 1718 cm^{-1} in the metastable form, the C1=O4 stretch that shifts from 1656 cm^{-1} for the amorphous form to 1648 cm^{-1} in the metastable form, and the band shift from 1421 to 1415 cm^{-1} which can be assigned to a deformation of a benzene ring (C2, C3, C4, C6, C9, C11; see Fig. 1) and stretching vibrations at adjacent single bonds (C1–C9 and C2–O3). These changes represent significant conformational and/or intermolecular bonding changes upon crystallization to the metastable form. In agreement with the conformational analysis these results indicate that the conformational orientation of the two benzyl rings, that are connected through C1, and the conformation of the aliphatic part of the molecule change during formation of the metastable crystalline form of fenofibrate. In molecules which exhibit strong interactions (e.g., hydrogen bonding) or conformers with a higher energetic barrier to conversion, structural characteristics have been described based on the vibrational spectra and quantum chemical calculations [26]. However, it is not possible in the case of fenofibrate to propose specific conformations or intermolecular interactions in the metastable form because the intermolecular interactions between fenofibrate molecules are rather weak. Upon polymorphic conversion to the stable crystalline form I many of the peak positions increase back to positions more similar to those for the amorphous form (in both the solid and liquid melt). Hence, it seems likely that the metastable and stable forms have different molecular conformations, and that the average molecular conformation in the amorphous form (both solid and liquid melt) is closer to that of the stable form; however solving the crystal structure would be required to confirm this hypothesis.

Further differences between the three solid-state forms and the melt of fenofibrate can be observed in the CH-stretching region between 2900 and 3200 cm^{-1} in particular involving symmetric and asymmetric stretches of CH groups at C15, C16, C19, and C20. These results once more indicate that changes in the aliphatic region of the fenofibrate molecule as well as the single bonds around C1 occur during the solid-state transformations upon recrystallization of amorphous fenofibrate.

To study the nature of the solid-state conversions in fenofibrate more closely and to obtain information about the structure of the solid-state forms occurring during the recrystallization of amorphous fenofibrate, the experimental Raman spectra were analyzed using multivariate analysis, namely, PCA. Furthermore, the results of the quantum chemical calculations were used to assign spectral bands to molecular vibrations that exhibited changes, thereby providing a deeper insight into structural changes in fenofibrate upon heating. The PCA model obtained after pre-treatment of the spectral data by SNV correction and mean centering explained 92.2 % of the spectral variation with the help of two principal components (PCs). According to the loadings plot (Fig. 8A), which visualizes the spectral variation between the different solid-state forms, the 1st PC is positively correlated with the spectral features of crystalline form I (peaks at 1147, 1588, 1728 cm^{-1}) and crystalline form II (peaks at 1598, 1648, 1718 cm^{-1}) and negatively correlated with the amorphous forms (dips at 1150, 1602, 1656 cm^{-1}) (Fig. 6). Thus, the largest spectral variation occurs between the amorphous and crystalline forms. The 2nd PC is more difficult to interpret and it is likely that several factors influence the loadings. However, it

Table 3
Spectral differences in the Raman spectra of different solid-state forms of fenofibrate occurring upon heating amorphous fenofibrate

Band assignment	Peak position/cm^{-1}			
	Amorphous form	Metastable crystalline form II	Stable crystalline form I	Melt
C16–O3 stretch, CH3 bending (C12, C17)	1150	1148	1147	1150
In-plane benzene ring stretch (C2, C3, C4, C6, C9, C11): Kekulé mode	1307/1316 (merged double band)	1303	1307	1307
In-plane benzene ring deformation (C2, C3, C4, C6, C9, C11), C1–C9 & C2–O3 bending	1421	1415	1421	1421
In-plane benzene ring stretch (C2, C3, C4, C6, C9, C11)	1600	1598	1599	1599
C1=O4 carbonyl stretch	1656	1648	1650	1655
C15=O2 carbonyl stretch	1730	1718	1728	1725

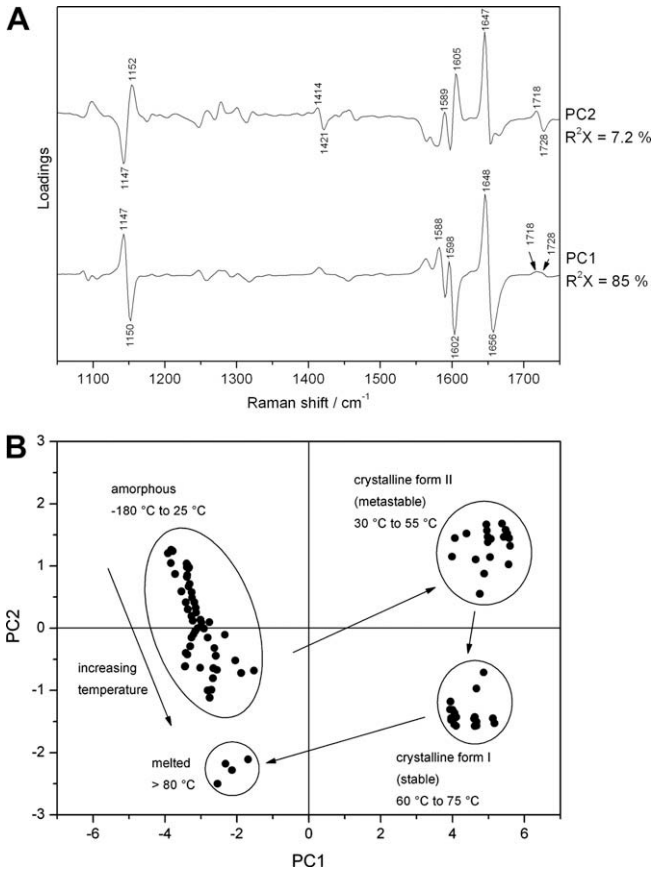

Fig. 8. Loadings (A) and scores (B) plots generated by PCA from the Raman spectra obtained upon heating amorphous fenofibrate between −180 and 90 °C. Loadings are offset for clarity.

becomes clear from both the loadings (Fig. 8A) and the scores plot (Fig. 8B) that the 2nd PC loadings are positively correlated with the crystalline form II (peaks at 1414 and 1718 cm^{-1}) and amorphous fenofibrate (peak at 1152 cm^{-1}), as well as negatively correlated with crystalline form I (peaks at 1421 and 1728 cm^{-1}).

In addition to the first two PCs, higher PCs and the difference between the model and the original data (DModX) were analyzed to obtain further information about the different solid-state forms of fenofibrate. While the PCA scores plot shows variation which contributes to the model, the DModX explains the residuals of the spectra to the model. The 3rd PC explains 4.8 % of the spectral variation and describes spectral differences similar to those described by the 2nd PC (data not shown). The DModX showed slightly higher residuals for the higher temperature samples. Higher PCs mainly describe noise and spectral variation of less than 1.4% and have hence not been included into the PCA model.

The scores plot in Fig. 8B shows separate clusters for the three solid-state forms and melted fenofibrate. The 1st PC separates the two ordered crystalline polymorphs on the one hand from the disordered amorphous and melted fenofibrate on the other hand. The 2nd PC allows the distinction between the two disordered forms, amorphous fenofibrate and the melt of the drug, which clearly form separate clusters. The spreading and decreasing scores values in the cluster of amorphous fenofibrate indicate a gradual increase of molecular mobility within the amorphous material with increasing temperature until the crystallization to the metastable crystalline form occurs at 30 °C and a separate cluster is formed. In addition to a separation between the two disordered forms, the 2nd PC separates crystalline form I from crystalline form II.

4. Conclusions

Quantum mechanical calculations were successfully used to investigate the vibrational spectra and the structure of crystalline and amorphous fenofibrate. Comparing the experimental spectra of crystalline and amorphous fenofibrate with the predicted spectra of a monomer and two dimer structures revealed that structural differences between crystalline and amorphous fenofibrate occur in aliphatic parts of the fenofibrate molecule around single bonds. The spectroscopic analysis suggests that non-hydrogen-bonded drug molecules such as fenofibrate are likely to exhibit random molecular orientations and conformations in the amorphous phase since the weak intermolecular interactions that occur between such molecules can easily be disrupted. *In situ* temperature-dependent Raman spectroscopy was used together with PCA for the first time to investigate the recrystallization of an amorphous pharmaceutical compound. Multiple solid-state forms, including the metastable crystalline form, could be observed and their structures were analyzed with the help of multivariate analysis and the results of the quantum chemical calculations. The study shows that vibrational spectroscopy combined with quantum chemical modeling and chemometrics is a useful combination to improve the molecular-level understanding of structural properties and physical behavior of different solid-state forms of pharmaceutical compounds.

Acknowledgements

The University of Otago (University of Otago Postgraduate Scholarship) and the Finnish Centre for International Mobility (CIMO) are acknowledged for financial support (A.H.). Damian Walls is acknowledged for help with the XRPD measurements. Dr. S. Howell is thanked for help with the quantum chemical calculations and Dr. Ch. Schmelzer for helpful comments.

References

[1] H.G. Brittain (Ed.), Polymorphism in pharmaceutical Solids, vol. 95, Marcel Dekker, Inc., New York, 2000.
[2] B. Rodríguez-Spong, C.P. Price, A. Jayasankar, A.J. Matzger, N. Rodriguez-Hornedo, General principles of pharmaceutical solid polymorphism: a supramolecular perspective, Adv. Drug Delivery Rev. 56 (2004) 241–274.
[3] S.R. Byrn, Solid-State Chemistry of Drugs, SSCI, Inc., West Lafayette, Indiana, 1999.
[4] L. Yu, Amorphous pharmaceutical solids: preparation, characterization and stabilization, Adv. Drug Delivery Rev. 48 (2001) 27–42.
[5] B.C. Hancock, G. Zografi, Characteristics and significance of the amorphous state in pharmaceutical systems, J. Pharm. Sci. 86 (1997) 1–12.
[6] D.Q.M. Craig, P.G. Royall, V.L. Kett, M.L. Hopton, The relevance of the amorphous state to pharmaceutical dosage forms: glassy drugs and freeze dried systems, Int. J. Pharm. 179 (1999) 179–207.
[7] S.R. Vippagunta, H.G. Brittain, D.J.W. Grant, Crystalline solids, Adv. Drug Delivery Rev. 48 (2001) 3–26.
[8] H.G. Brittain (Ed.), Physical Characterization of Pharmaceutical Solids, vol. 70, Marcel Dekker, Inc., New York, 1995.
[9] J.A. Zeitler, P.F. Taday, D.A. Newnham, M. Pepper, K.C. Gordon, T. Rades, Terahertz pulsed spectroscopy and imaging in the pharmaceutical setting – a review, J. Pharm. Pharmacol. 59 (2007) 209–223.
[10] C.M. McGoverin, L.C.H. Ho, J.A. Zeitler, C.J. Strachan, K.C. Gordon, T. Rades, Quantification of binary polymorphic mixtures of ranitidine hydrochloride using NIR spectroscopy, Vibr. Spectrosc. 41 (2006) 225–231.
[11] J. Aaltonen, K. Kogermann, C.J. Strachan, J. Rantanen, In-line monitoring of solid-state transitions during fluidisation, Chem. Eng. Sci. 62 (2007) 408–415.
[12] A. Tudor, S. Church, P. Hendra, M. Davies, C. Melia, The qualitative and quantitative analysis of chlorpropamide polymorphic mixtures near-infrared Fourier transform Raman spectroscopy, Pharm. Res. 10 (1993) 1772–1776.
[13] C.M. Deeley, R.A. Spragg, T.L. Threlfall, A comparison of Fourier-transform infrared and near-infrared Fourier-transform Raman-spectroscopy for quantitative measurements – an application in polymorphism, Spectrochim. Acta A Mol. Biomol. Spectrosc. 47 (1991) 1217–1223.
[14] C.J. Strachan, D. Pratiwi, K.C. Gordon, T. Rades, Quantitative analysis of polymorphic mixtures of carbamazepine by Raman spectroscopy and principal components analysis, J. Raman Spectrosc. 35 (2004) 347–352.

[15] C.J. Strachan, T. Rades, D.A. Newnham, K.C. Gordon, M. Pepper, P.F. Taday, Using terahertz pulsed spectroscopy to study crystallinity of pharmaceutical materials, Chem. Phys. Lett. 390 (2004) 20–24.
[16] C.G. Kontoyannis, N.C. Bouropoulos, P.G. Koutsoukos, Use of Raman spectroscopy for the quantitative analysis of calcium oxalate hydrates: application for the analysis of urinary stones, Appl. Spectrosc. 51 (1997) 64–67.
[17] L.S. Taylor, G. Zografi, The quantitative analysis of crystallinity using FT-Raman spectroscopy, Pharm. Res. 15 (1998) 755–761.
[18] L.S. Taylor, G. Zografi, Spectroscopic characterization of interactions between PVP and indomethacin in amorphous molecular dispersions, Pharm. Res. 14 (1997) 1691–1697.
[19] S. Söderholm, Y. Roos, N. Meinander, M. Hotokka, Raman spectra of fructose and glucose in the amorphous crystalline states, J. Raman Spectrosc. 30 (1999) 1009–1018.
[20] W.P. Findlay, D.E. Bugay, Utilization of Fourier transform Raman spectroscopy for the study of pharmaceutical crystal forms, J. Pharm. Biomed. Anal. 16 (1998) 921–930.
[21] C.J. Strachan, S.L. Howell, T. Rades, K.C. Gordon, A theoretical and spectroscopic study of carbamazepine polymorphs, J. Raman Spectrosc. 35 (2004) 401–408.
[22] C.J. Strachan, T. Rades, K.C. Gordon, A theoretical and spectroscopic study of gamma-crystalline and amorphous indometacin, J. Pharm. Pharmacol. 59 (2007) 261–269.
[23] J. Foresman and Æ. Frisch, Exploring chemistry with electronic structure methods, Gaussian, Inc., Pittsburgh, 1995–1996, pp. 302.
[24] K.C. Gordon, C.M. McGoverin, C.J. Strachan, T. Rades, The use of quantum chemistry in pharmaceutical research as illustrated by case studies of indometacin and carbarnazepine, J. Pharm. Pharmacol. 59 (2007) 271–277.
[25] G.M. Day, J.A. Zeitler, W. Jones, T. Rades, P.F. Taday, Understanding the influence of polymorphism on phonon spectra: lattice dynamics calculations and terahertz spectroscopy of carbamazepine, J. Phys. Chem. B 110 (2006) 447–456.
[26] M.M. Nolasco, A.M. Amado, P.J.A. Ribeiro-Claro, Computationally-assisted approach to the vibrational spectra of molecular crystals: study of hydrogen-bonding and pseudo-polymorphism, Chem. Phys. Chem. 7 (2006) 2150–2161.
[27] C.J. Strachan, S.L. Howell, A. Heinz, T. Rades and K.C. Gordon, Insight into the short-range order of amorphous pharmaceutical materials with hydrogen bonding capability using vibrational spectroscopy and computational chemistry, AAPS Annual Meeting and Exposition, San Diego, USA, 2007.
[28] K. Kogermann, J. Aaltonen, C.J. Strachan, K. Pollanen, P. Veski, J. Heinamaki, J. Yliruusi, J. Rantanen, Qualitative in situ analysis of multiple solid-state forms using spectroscopy and partial least squares discriminant modeling, J. Pharm. Sci. 96 (2007) 1802–1820.
[29] J. Aaltonen, P. Heinanen, L. Peltonen, H. Kortejarvi, V.P. Tanninen, L. Christiansen, J. Hirvonen, J. Yliruusi, J. Rantanen, In situ measurement of solvent-mediated phase transformations during dissolution testing, J. Pharm. Sci. 95 (2006) 2730–2737.
[30] C.J. Lee, C. Rawle, C.J. Strachan, T. Rades, P. Manson, K. Payne, Method and Apparatus for Performing a Second Order Non-Linear Optical Measurement on a Sample, New Zealand Patent Office, New Zealand, 2004.
[31] M. Savolainen, A. Heinz, C. Strachan, K.C. Gordon, J. Yliruusi, T. Rades, N. Sandler, Screening for differences in the amorphous state of indomethacin using multivariate visualization, Eur. J. Pharm. Sci. 30 (2007) 113–123.
[32] A.C. Jørgensen, I. Miroshnyk, M. Karjalainen, K. Jouppila, S. Siiria, O. Antikainen, J. Rantanen, Multivariate data analysis as a fast tool in evaluation of solid state phenomena, J. Pharm. Sci. 95 (2006) 906–916.
[33] R.F. Henry, G.Z. Zhang, Y. Gao, I.S. Buckner, Fenofibrate, Acta Crystallogr. Sect. E 59 (2003) O699–O700.
[34] P. Di Martino, G.F. Palmieri, S. Martelli, Evidence of a metastable form of fenofibrate, Pharmazie 55 (2000) 625–626.
[35] D.L. Zhou, G.G.Z. Zhang, D. Law, D.J.W. Grant, E.A. Schmitt, Physical stability of amorphous pharmaceuticals: importance of configurational thermodynamic quantities and molecular mobility, J. Pharm. Sci. 91 (2002) 1863–1872.
[36] B.J. Matthewson, A. Flood, M.I.J. Polson, C. Armstrong, D.L. Phillips, K.C. Gordon, Vibrational spectra of Dipyrido[3,2-a:2′,3′-c]phenazine and its radical anion analyzed by ab initio calculations and deuteration studies, Bull. Chem. Soc. Jpn. 75 (2002) 933–942.
[37] K.C. Gordon, A.K. Burrell, T.J. Simpson, S.E. Page, G. Kelso, M.I.J. Polson, A. Flood, Probing the nature of the redox products and lowest excited state of (bpy)(2)Ru(mu-bptz)Ru(bpy)(2) (4+): a resonance Raman study, Eur. J. Inorg. Chem. (2002) 554–563.
[38] M.J. Frisch, G.W. Trucks, H.B. Schlegel, G.E. Scuseria, M.A.C. Robb, J. R., J. Montgomery, J. A., T. Vreven, K.N. Kudin, J.C. Burant, J.M. Millam, S.S. Iyengar, J. Tomasi, V. Barone, B. Mennucci, M. Cossi, G. Scalmani, N. Rega, G.A. Petersson, H. Nakatsuji, M. Hada, M. Ehara, K. Toyota, R. Fukuda, J. Hasegawa, M. Ishida, T. Nakajima, Y. Honda, O. Kitao, H. Nakai, M. Klene, X. Li, J.E. Knox, H.P. Hratchian, J.B. Cross, V. Bakken, C. Adamo, J. Jaramillo, R. Gomperts, R.E. Stratmann, O. Yazyev, A.J. Austin, R. Cammi, C. Pomelli, J.W. Ochterski, P.Y. Ayala, K. Morokuma, G.A. Voth, P. Salvador, J.J. Dannenberg, V.G. Zakrzewski, S. Dapprich, A.D. Daniels, M.C. Strain, O. Farkas, D.K. Malick, A.D. Rabuck, K. Raghavachari, J.B. Foresman, J.V. Ortiz, Q. Cui, A.G. Baboul, S. Clifford, J. Cioslowski, B.B. Stefanov, G. Liu, A. Liashenko, P. Piskorz, I. Komaromi, R.L. Martin, D.J. Fox, T. Keith, M.A. Al-Laham, C.Y. Peng, A. Nanayakkara, M. Challacombe, P.M.W. Gill, B. Johnson, W. Chen, M.W. Wong, C. Gonzalez, J.A. Pople, Gaussian 03, Revision C.02, Gaussian, Inc., Wallingford, CT, 2004.
[39] P.T. Lehtovuori, T.H. Nyrönen, SOMA – workflow for small molecule property calculations on a multiplatform computing grid, J. Chem. Inf. Model. 46 (2006) 620–625.
[40] T. Nyrönen, T. Kinnunen, P. Lehtovuori, Seamless computing across versatile IT infrastructures – SOMA drug discovery environment, CSC News (2006) 36–37.
[41] G.A. Guirgis, Y.E. Nashed, J.R. Durig, Infrared and Raman spectra, conformational stability, barriers to internal rotation, normal-coordinate calculations and vibrational assignments for vinyl silyl bromide, Spectrochim. Acta A Mol. Biomol. Spectrosc. 56 (2000) 1065–1078.
[42] A.P. Scott, L. Radom, Harmonic vibrational frequencies: an evaluation of Hartree–Fock, Moller–Plesset, quadratic configuration interaction, density functional theory, and semiempirical scale factors, J. Phys. Chem. 100 (1996) 16502–16513.